Artificial Bee and Ant Colony-assisted Performance Improvements in Artificial Neural Network-based Rotor Fault Detection

Osman Zeki Erbahan*, Ibrahim Aliskan
Department of Electrical-Electronics Engineering, Faculty of Engineering, Bulent Ecevit University, Zonguldak, Turkey,
ozeki.erbahan@fbe.karaelmas.edu.tr

***Abstract*—Asynchronous motors are the most commonly used types of motor in the industry. They are preferred because of their ease of control and reasonable cost. Since it is not desirable to suspend production in factories, it is required that motor failures used in production lines be detected quickly and easily. In this article, sound signals were recorded during the operation of the asynchronous motor, which is operational and with a rotor bar crack; and filtering, normalization, and Fast Fourier Transform were performed. The detection of rotor broken bar error was examined using the feed-forward backpropagation Artificial Neural Network (ANN) method. With intuitive algorithms such as the artificial bee colony and artificial ant colony, improvements to the ANN results were investigated. The experimental results verified that intuitive algorithms can improve the estimation performance of the neural network.**

***Index Terms*—Ant colony algorithm; Artificial neural networks; Bee colony algorithm; Induction motor; Rotor bar crack.**

I. INTRODUCTION

Asynchronous motors, which have important features such as cost effectiveness, easy speed control, low maintenance cost, and low maintenance requirement, are used in most production lines. Stator and rotor failures and, generally, mechanical failures can be seen in these motors. These failures must be detected during operation or in advance. In this way, by providing the proper operating conditions, the production system is prevented from being disrupted.

An Artificial Neural Network (ANN) is a structure based on a human learning mechanism. ANNs have been used in the diagnosis of motor failures based on learning ability. In many studies, detection methods related to asynchronous motor bearing and stator failures were examined [1], [2]. Glowacz and Glowacz [3] detected stator failures of a single-phase asynchronous motor that employs acoustic signals. In the article, the sound signals of the one-phase asynchronous motor were examined through ANNs and the short circuit fault detection in the stator windings were analyzed. The comparison was made by using three different ANN methods. Delgado-Arredondo, Morinigo-Sotelo, Osornio-Rios, Avina-Cervantes, Rostro-Gonzalez, and Romero-Troncoso [4] examined a method known as motor current analysis, which identifies errors in asynchronous motors through sound and vibration signals. In this article, the error detection methodology was examined by acoustic signals in squirrel-cage induction motors. The study was carried out to detect rotor bar fractures, mechanical imbalances, and bearing defects in the motors. Khater, El-Sebah, Osama, and Sakkoury [5] created a special model for the detection of rotor fractures of the asynchronous motor driven by an alternating current (AC) driver. They examined the determination of the number of broken rotor bars of the asynchronous motor. In a model-based study [6], alterations in three-phase currents were observed to diagnose rotor fractures and bearing failures of induction motors. Asad, Vaimann, Belachen, Kallaste, Rassölkin, and Iqbal [7] used the applied voltage variations on the motor to determine the broken rotor bar of the motor, whose torque was controlled by an inverter. The study revealed the results that the method was effective. Deus, Sobrinho, Belo, Brito, de Souza Ramos, and Lima-Filho [8] reported a less costly method than conventional methods by analyzing the stator current values of the asynchronous motor, detecting broken rotor bar failures at different levels. Garcia-Calva, Morinigo-Sotelo, Garcia-Perez, Camarena-Martinez, and Romero-Troncoso [9] obtained results in the detection of broken rotor rod failure of inverter-driven motors by analyzing current harmonicity. Dias, da Silva, and Alves [10] detected broken rotor bars in AC motors, which brought up a new approach depending on current analysis. Soleimani, Cruz, and Haghjoo [11] reported a method for the detection of broken rotor bars in AC motors based on the examination of the air gap magnetic field between the stator and the rotor. Elez, Car, Tvoric, and Vaseghi [12] added two coils to the motor stator to measure the field change in the air gap. Magnetic field changes obtained by these coils were shown to detect rotor bar fractures in the motor. Gritli, Rossi, Casadei, Filippetti, and Capolino [13] examined the active and reactive powers of a three-phase winding rotor induction motor, and detected electrical faults of the rotor with rotor spectral current and voltage values. In the study in [14], before applying the monitoring methods based on the current analysis, the

Manuscript received 12 January, 2022; accepted 11 February, 2022.

presence of various harmonics in healthy machines was thoroughly analyzed, the harmonics of the rotor fractures were compared, and the failure was detected. Keskes and Braham [15] achieved highly accurate results in the detection of broken rotor bar failures, which are very close to the main frequency in the spectrum and difficult to realize, with both wavelength package conversion and a graphic support vector combination. The authors in [16] performed the detection of rotor bar semi-fracture by applying multiple signal analysis to the stator current signal with a Kalman filter. St-Onge, Cameron, Saleh, and Scheme [17] detected rotor rod fracture using the attribute extraction method with pattern-based diagnostics in three-phase asynchronous motors. Trachi, Elbouchikhi, Choqueuse, and Benbouzid [18] detected broken bearings and rotor bars using a high-resolution spectral analysis technique based on stator current measurements. Xu *et al.* [19] achieved positive results using the multi-feature extraction method in winding short circuit detection in motors. Ramu, Irudayaraj, Subramani, and Subramaniam [20] proposed a new approach to detect broken rotor bar failures using Hilbert Transform and ANN when the asynchronous three-phase motor is controlled by a motor driver. Wang, Liu, Guo, and Wang [21] conducted a study of engine error analysis using the noise-based incomplete wavelet packet analysis - ANN model in gasoline engines.

When all these studies are examined, it is seen that the usage of ANN has increased in recent years in the detection of motor failures. And in this study, it is mainly proposed how the diagnostic performance of the ANN can be improved by employing intuitive algorithms. If the literature is examined, it is seen that no optimization process was performed during the submission of input data to the neural network [3], [20]–[23]. If metaheuristic optimization algorithms are viewed, it is seen that Artificial Bee Colony (ABC) and Artificial Ant Colony (AAC) algorithms have a simple and flexible structure [24]. They also provide ease of use for discrete problems. Therefore, in this study, the data set to be submitted to ANN was reordered using ABC and AAC algorithms, and the estimation performance of ANN was improved.

In this study, audio signs of a three-phase induction machine with healthy and broken rotor bars were recorded. Noises were minimized by employing the windowing method. Fast Fourier Transformation (FFT) was applied to the filtered signs. The resulting samples were applied to the feed-forward backpropagation ANN, and the rotor crack detection performance of the developed ANN was examined. After that, the data order was arranged using the artificial ant and bee colony algorithms. Data were ordered by calculating the shortest distance in artificial ant optimization and determining the best source of artificial bee colony optimization. New weights were obtained by training the ANN with the input data set that had been reordered with the ABC algorithm or the AAC algorithm.

The explanations on experimental results, intuitive-assisted ANN details, performance, and evaluation, and ultimately the results, are presented in the following sections of the article, respectively.

II. ARTIFICIAL NEURAL NETWORKS

An ANN consists of a series of interconnected processing elements called “neurons”. A general view of the multilayered ANN structure, which is selected for employing in this study, is given in Fig. 1.

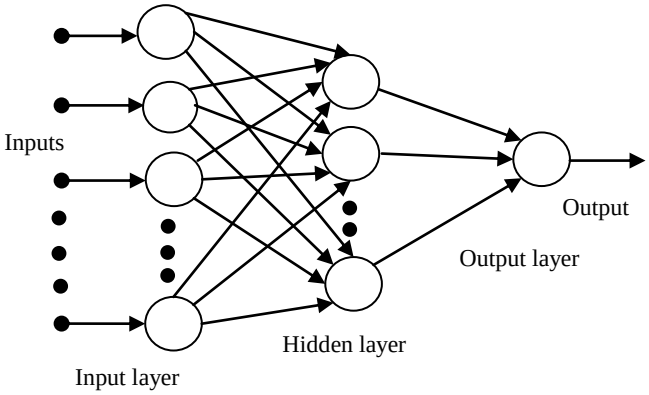

Fig. 1. Overview of the ANN.

The general representation of an artificial neuron is presented in Fig. 2. In this topology, the outputs of the neurons in the previous layer are taken as input parameters to the neurons in the next layer. And in the neuron, the input parameter is multiplied by its own weight value and incorporated into the operations. The neuron collects these weighted signals and its threshold value. In a classical neuron structure, the neuron runs its activation function with the total result. Finally, it sends the output of the transfer function to the neurons of the next layer.

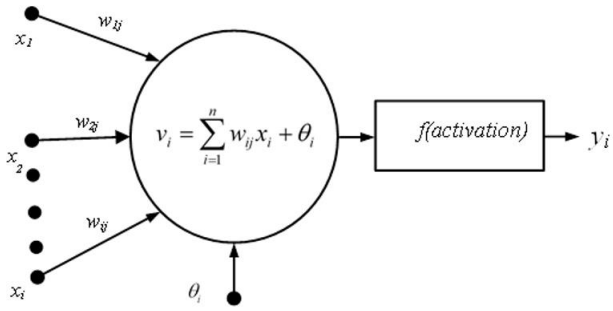

Fig. 2. The structure of the classical neuron.

The relationship between the input signals and the output signal of a neuron is defined as

$$y_j = f\left(\sum_{i=1}^{n}\left(x_i * w_{ij}\right) + \theta_j\right), \tag{1}$$

where y_j is the output value of the jth neuron, x_i is the ith input value, w_{ij} is the weight value of the connection between the jth neuron and the ith input, θ_j is the threshold value of the jth neuron, n is the number of inputs, and f is the activation function used.

Transfer functions such as the logarithmic sigmoids below can be preferred, since solutions to nonlinear problems are sought using ANNs. Furthermore, neuron function was selected as sigmoid as the output value would be in the range of 0 to 1 in this study

$$f(x)=\frac{1}{1-e^{-x}}. \quad (2)$$

The input signals are normalized to be compatible with the operating range of the selected transfer function. Denormalization is performed on the attained output signals; however, denormalization is not needed in this study.

To obtain the estimation ability, the ANN must undergo the training phase. In the training phase, the weight and threshold values are updated at each iteration, depending on the estimation error. In this study, the ANN parameters (weights and thresholds) are updated by performing the backpropagation algorithm which is given in detail in [25]. According to the termination criterion, the optimization process is stopped. The iteration number or the estimation performance can be chosen as the stopping criterion. Here, the iteration number is applied as a stopping criterion for the training.

III. THE ARTIFICIAL BEE COLONY ALGORITHM

The ABC algorithm was developed by modeling the behavior of bees searching for food in the natural world [24], [26]. It is accepted that the number of bees involved in this algorithm will be equal to the number of food sources available. In the algorithm, the bee colony is considered to consist of three different classes of bees: worker bees, onlooker bees, and scout bees. It is assumed that half of the colony are worker bees and the other half are onlooker bees. The scout bee, on the other hand, represents status and can be described as a temporary phase in which the worker bee, which is running out of food supply, randomly searches for a source of food. The worker bee, which runs out of nectar, turns into a scout bee. The algorithm uses the following equation to produce initial food sources

$$x_{ij}=x_j^{\min}+rand(0,1)(x_j^{\max}-x_j^{\min}), \quad (3)$$

where *i: 1... SN* and *j: 1... D*. Here, *SN* is the number of food sources and *D* is the number of parameters to optimize. The lower limit of the j[th] parameter is $x_j^{\min}$ and the upper limit of the *j*th parameter is $x_j^{\max}$.

Each source has a worker bee. Therefore, the number of food sources and the number of worker bees are equal. The simulation to determine the new resource in the existing resource neighborhood is defined by the expression given in (4)

$$v_{ij}=x_{ij}+\varphi_{ij}(x_{ij}-x_{jk}), \quad (4)$$

where *j* is a randomly selected value in the range of *1... D*. *k* is a number selected in the range of *1... SN*, and must be a number taking a value between $\varphi_{ij} \in$ [-1, 1].

If these generated values exceed the previously determined parameters, the values will be offset according to the following formula

$$v_{ij}=\begin{cases} x_j^{\min}, & v_{ij}<x_j^{\min}, \\ v_{ij}, & x_j^{\min}\le v_{ij}\le x_j^{\max}, \\ x_j^{\max}, & v_{ij}>x_j^{\max}. \end{cases} \quad (5)$$

The conformity value of the new resource found is presented as follows

$$fitness_i=\begin{cases} \frac{1}{1+f_i}, & f_i\ge 0, \\ 1+abs(f_i), & f_i<0, \end{cases} \quad (6)$$

where f_i is the cost value of the v_i resource that is the solution.

After completing their research in one cycle, all worker bees return and transfer the nectar information of the nectar sources they find to the onlooker bees in the form of dances. This is done using the conformity value. For this, the roulette wheel method is used. According to the roulette wheel method, the more the same option is in the areas on the rotating wheel, the more likely the arrow will point with that option.

All conformity values are collected and formulated with a larger place on the wheel for those with good conformity values.

The ratio of a resource's conformity value to the sum of the conformity value of all resources gives that resource's likelihood of being selected relative to other resources

$$p_i=\frac{fitness_i}{\sum_{j=1}^{SN} fitness_j}, \quad (7)$$

where $fitness_i$ is the quality of resource *i*, *SN* is the number of worker bees.

After the probability values are calculated in the algorithm, a random number is produced in the range of [0, 1] for each resource in the selection process according to the roulette wheel using these values. And if the value of p_i is greater than the number produced, onlooker bees also produce a new solution, such as worker bees, in this resource region by using (4).

The new solution is evaluated and its quality is calculated. The new and old solutions are compared and the optimal one is selected. This process continues until all onlooker bees spread to food areas.

At the end of a cycle, when all worker and onlooker bees complete the search process, the worker bee in the finished resource now becomes a scout bee and randomly initiates the new resource search process, as given in (3).

The optimization process continues until the termination criterion is reached. In this study, the number of iterations is chosen as the termination criterion.

IV. THE ARTIFICIAL ANT COLONY ALGORITHM

Animals that live in colonies and solve their problems through cooperation are described as social animals. Ants are also animals that fall into this group [27]. The AAC algorithm is an algorithm based on mathematical models of real ant behavior. However, the difference from artificial ants is that they have a certain memory, are not completely blind, and live in a discrete-time environment. This algorithm yields good results in the solution of the traveler seller problem, which is widely used in the literature [28].

This problem consists of creating a closed tour with a minimum distance, provided that the seller visits each of the n number of cities once. Let d_{ij} be the distance between cities i and j

$$d_{ij} = \left[(x_i - x_j)^2 + (y_i - y_j)^2 \right]^{1/2}. \quad (8)$$

If m indicates the number of ants in the colony, and $b_i(t)$ gives the number of ants at moment t, then (9) can be presented

$$m = \sum_{i=1}^{n} b_i(t). \quad (9)$$

If $\tau_{ij}(t)$ indicates the amount of pheromone substance stored in the line (i, j) between i and j, the pheromone substance at moment $t + 1$ is given as below

$$\tau_{ij}(t+1) = \rho \tau_{ij}(t) + \Delta \tau_{ij}(t, t+1), \quad (10)$$

where ρ is the evaporation rate. The amount of pheromone delivered in per unit time is calculated as

$$\Delta \tau_{ij}(t, t+1) = \sum_{k=1}^{n} \Delta \tau_{ij}^{k}(t, t+1). \quad (11)$$

For an ant, the heuristic information controlling the move from ith city to jth city is shown as follows

$$\eta_{ij} = \frac{1}{d_{ij}}. \quad (12)$$

Finally, the moving probability for the kth ant from ith city to jth city is presented in (13)

$$P_{ij}(t) = \begin{cases} \dfrac{[\tau_{ij}(t)]^{\alpha} [\eta_{ij}]^{\beta}}{\sum_{j \in N_i^k} [\tau_{ij}(t)]^{\alpha} [\eta_{ij}]^{\beta}}, & if \ j \in N_i^k, \\ 0, & otherwise. \end{cases} \quad (13)$$

Above α and β are two positive real parameters that specify the relative influence of the pheromone trail and the heuristic information. For the kth ant when it is at the ith city, N_i^k is the set of cities in the taboo list that has not been visited yet. A taboo list is prepared for each ant to visit n number of cities. When the tour is completed, this taboo list is reset too.

For this study, in the optimization study with the artificial ant colony algorithm, the distances between the spectral distribution points of each sign were taken into account and the shortest distance was calculated. The feed-forward backpropagation algorithm for the shortest distance values was reapplied to find the best solutions and new error values were given.

V. EXPERIMENTAL STUDY FOR ROTOR FAILURE DETECTION

The recorded motor sound signals for the detection of rotor bar fractures are processed step by step in accordance with the block diagram given in Fig. 3.

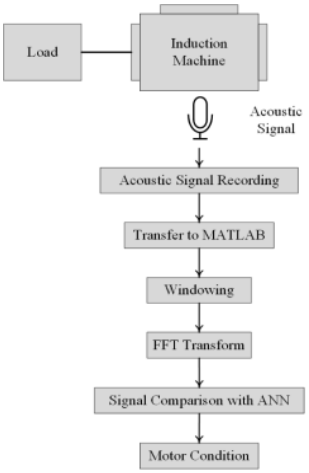

Fig. 3. Block diagram representation for stages of the study.

Sound measurements made around the motor at various speeds and loads are taken in a laboratory environment and stored as data. Both for the healthy motor and for the motor where the rotor failure is created, these measurements are repeated and the audio data are transferred to the Matlab software.

The windowing method was used to filter sound signals. After some trials, the number of windows taken as 80. Figures 4(a) and 5(a) show raw audio data. A new signal was obtained by taking the arithmetic average of the 80 subparts of recorded audio data. Figures 4(b) and 5(b) show sound signals after the windowing process. The FFT transform of this resulting signal was performed, and the spectrums given in Fig. 4(c) and Fig. 5(c) were obtained.

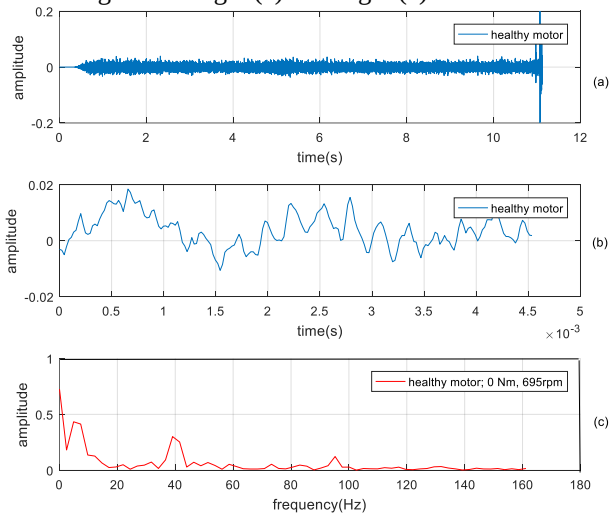

Fig. 4. (a) Audio recording for the healthy motor; (b) Audio data obtained after windowing; (c) Spectrum change after FFT application.

Spectral changes are obtained by using the FFT. Here, the number of spectral lines is 84, the bandwidth (f_{max}) is 200 Hz and the frequency resolution (Δf) is 2.37 Hz. The sampling frequency (f_s) was taken as 44 kHz and the block size (N) was 4096 in the time domain. In this study, to detect the faulty motor, the specific spectrum area, which includes the signals with an amplitude greater than 0.05, is considered.

Figure 6 shows the spectrums selected for the healthy motor and faulty motor. This operation was applied to all

signals.

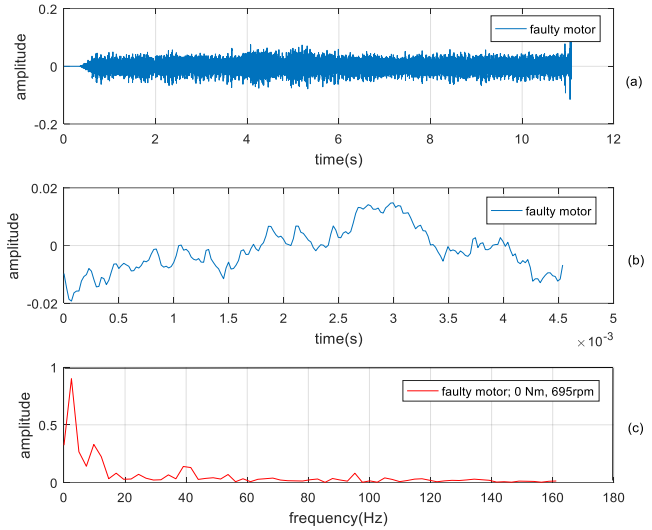

Fig. 5. (a) The audio recording for the faulty motor; (b) Audio data obtained after windowing; (c) Spectrum change after FFT application.

The harmonics presented in Fig. 6 were normalized with regard to main omponent and switched to comparison processes.

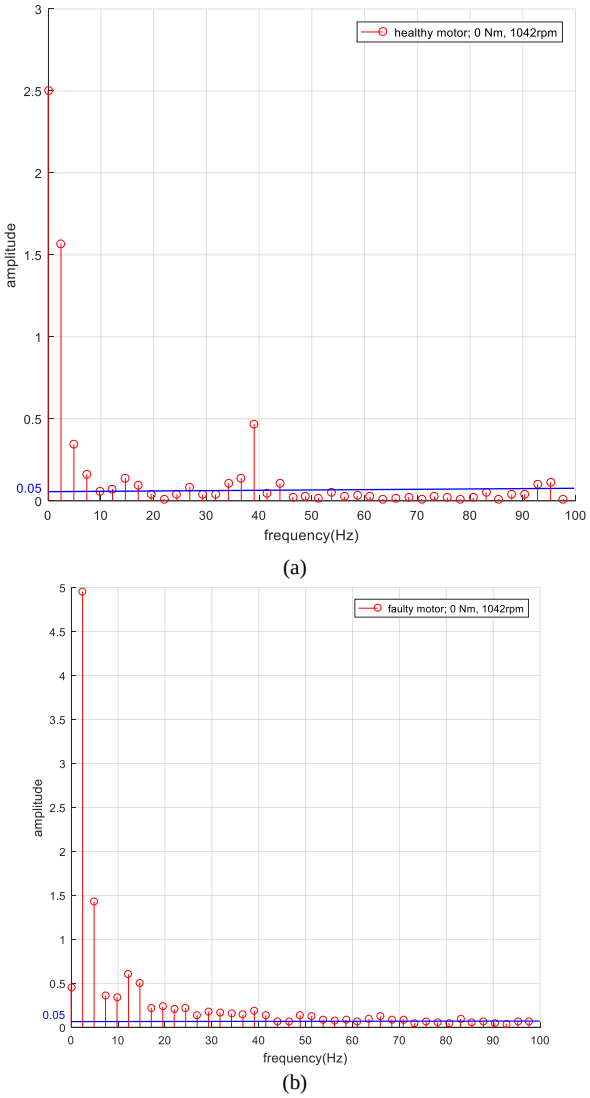

Fig. 6. (a) Spectrum selection of the healthy motor and (b) faulty motor. The amplitude value of 0.05 is the choice criterion.

A brief info about the experimental setup can be helpful to talk the laboratory studies. A 3-phase 0.25 kW 1390 rpm, 380 V AC, 0.8 A squirrel cage asynchronous motor was used. An image of the motor examined is given in Fig. 7.

Fig. 7. The motor used in the test.

AC Driver: An ABB brand ACS150 model driver of 0.37 kW power was used as an AC driver to perform acoustic measurement at various speeds of the motor in the test circuit. A K&H brand, EM3320-1. A model magnetic braking unit was used to get acoustic measurements of the motor under load.

Microphone: A condenser-type microphone was used for acoustic measurements. The sensitivity range of the microphone is between 100 Hz and 10 kHz.

To create the bar fracture, a 2 mm-diameter hole was drilled from the point where the aluminum short circuit bars of the rotor were located after the rotor was removed from the motor. The resulting space was closed with silicone to prevent it from creating undesirable sounds. Figure 8 shows the hole that was drilled into the rotor.

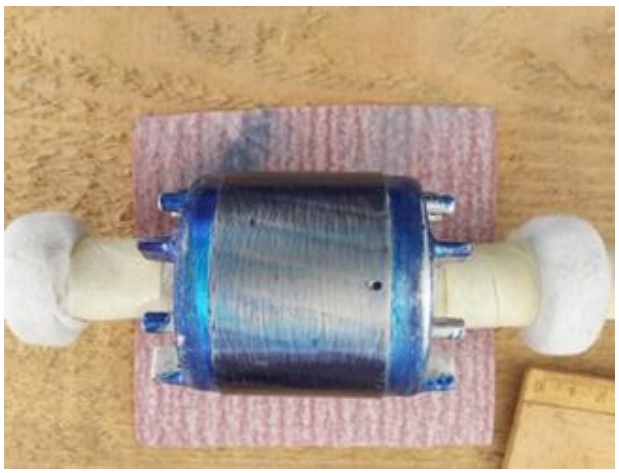

Fig. 8. Single bar broken in the rotor.

The motor was controlled by employing the AC driver. The motor was connected to the braking unit with the appropriate coupling. The microphone, located close to the body of the motor, was connected to the computer and audio files were recorded in *.m4a format.

While the speed of the motor was controlled by the driver, the change of load was adjusted in Nm via the braking controller. The motor was loaded at 0 % (no load),

25 %, 50 %, 75 %, 100 %, and 125 % of the nominal torque value. In the trials, it was observed that when the torque values increased in low-speed revolutions, the motor did not revolve and was locked. Therefore, a total of 54 data were recorded. In Table I, the data that cannot be recorded are shown with x. rses-i, i: 1, 2, ..., 30 are audio files recorded .

TABLE I. AUDIO FILES OBTAINED FOR DİFFERENT SPEEDS AND LOADS.

Torque **Speed**	**0 %** (*0 Nm*)	**25 %** (*0,42 Nm*)	**50 %** (*0,85 Nm*)	**75 %** (*1,28 Nm*)	**100 %** (*1,71 Nm*)	**125 %** (*2,14 Nm*)
25 % 347 rpm/	rses1	rses6	rses11	x	x	x
50 % 696 rpm	rses2	rses7	rses12	rses17	rses22	rses27
75 % 1042 rpm	rses3	rses8	rses13	rses18	rses23	rses28
90 % 1251 rpm	rses4	rses9	rses14	rses19	rses24	rses29
100 % 1390 rpm	rses5	rses10	rses15	rses20	rses25	rses30

The windowing method was applied in the Matlab software to filter the sound signal. FFT was performed for filtered audio data. For example, the spectrums obtained after the evaluation of the audio file of the motor with a solid rotor and the one with a single broken rotor bar with the Matlab are given in Figs. 9 and 10.

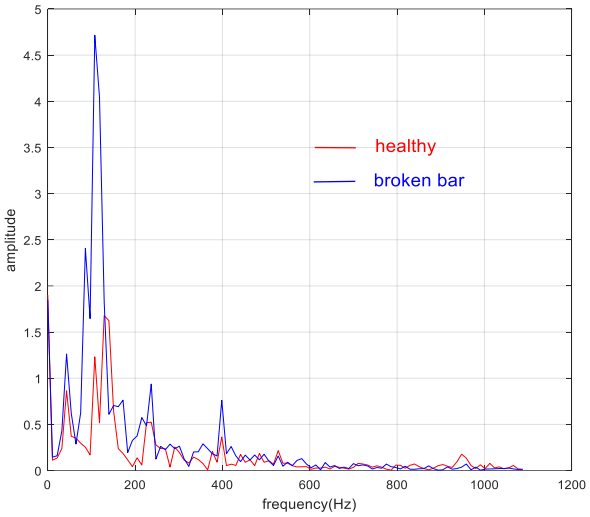

Fig. 9. The spectrums of the motor audio file of with a solid and broken rotor bar at 0 % torque (unloaded 0 Nm) and 100 % nominal speed (1390 rpm).

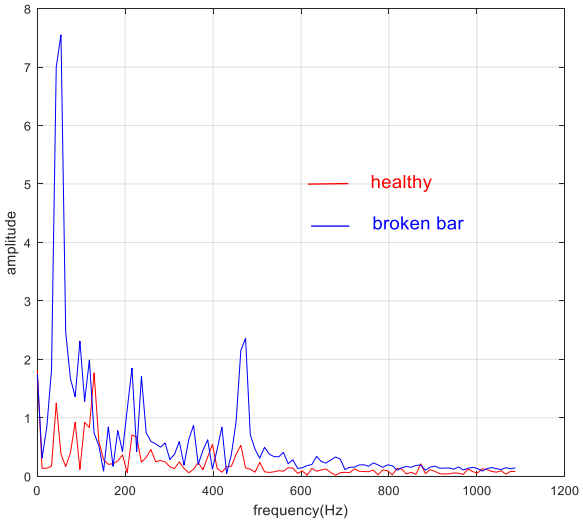

Fig. 10. The spectrums of the motor audio file with a solid and broken rotor bar at 125 % torque (2.146 Nm) and 100 % nominal speed (1390 rpm).

VI. DEVELOPMENT OF INTUITIVELY SUPPORTED ANN

Here, 44 data sets were used for training and 10 for testing. 22 of the 44 available data sets belong to the healthy motor, and the other 22 belong to the faulty motor.The first optimization study was performed using randomly ordered data sets. The second and third were made with data sets, which were ordered by ant colony and bee colony algorithms. The shortest distance value for the ant colony and the best source data for the bee colony algorithm were employed. The ABC algorithm usesm(3) to produce initial food sources [24]. The Mean Squared Error (MSE) is used as the performance index. Parameters for the ABC optimization algorithm: the number of food sources SN = 44 (number of data sets used for training steps), the number of parameters to optimize D = 45 (number of inputs from ANN), iteration number = 10, lower limit $x_j^{\min}$ = 1, upper limit $x_j^{\max}$ = 44. It is reminded that after a great number of trials, the values with the best results were taken as parameter values in the optimization work

$$MSE = \frac{1}{2}\sum_m E_m^2, \tag{14}$$

where m is the number of data sets, E_m is the estimation error

$$E_m = B_m - Q_m, \tag{15}$$

where B_m is the expected output (healthy motor: 1, faulty motor: 0), Q_m is the ANN output.

In the AAC algorithm, this problem consists of creating a closed tour with a minimum distance, provided that the seller visits each of the n numbers of cities once [27], [28]. Distance d_{ij} is calculated by employing (8). The distances between the spectral distribution points of each sign were taken into account and the shortest distance was calculated. The feedforward backpropagation algorithm for the shortest distance values was reapplied to find the best solutions, and new error values were given. The MSE is used as an error function. Parameters for the AAC optimization algorithm: ant number = 50, iteration number = 10, pheromone parameter α = 1, parameter for the heuristic information β = 1, evaporation rate δ = 0,5. These are the optimization

parameters determined with trial-error, which provide the best estimation results. The MSE changes through the optimization process for those two cases are presented in Figs. 11 and 12.

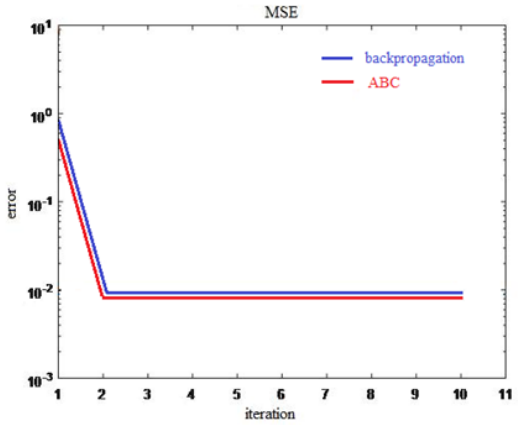

Fig. 11. The performance indices of ANN training for the case of ABC assistance.

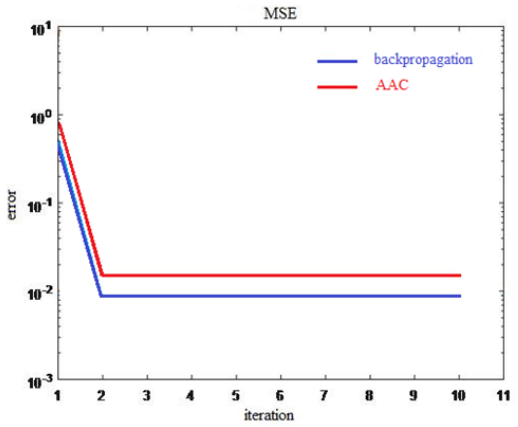

Fig. 12. The performance indices of ANN training for the case of AAC assistance.

In the figures, "backpropagation" shows the MSE of ANN with randomly ordered input data sets. "ABC" is the MSE variation of ABC-assisted ANN according to the iteration number, and "AAC" is the MSE variation of AAC-assisted ANN according to the iteration number.

VII. Performance Evaluation

In the feed forward back propagation algorithm model, in which 54 data points are used, 44 data points are used for training and 10 data points for testing. There are 45 inputs for ANN. The inputs have been selected by taking amplitudes greater than 0.05 as seen in Fig. 6. In the feed-forward backpropagation application with a single hidden layer with 10 neurons improved by an individual Matlab code, the test error rate was obtained as MSE of 0.0117872. At this step, a randomly ordered data set was used.

ANN training was done with input data set sorted by ABC algorithm. The same operations were performed for the data set sorted with the AAC algorithm. Then, test data were applied to both ANNs, and MSE values were calculated for each one. Now we have the MSE values of three different ANNs. These values are presented in Table II. In the table, ANN-E is the MSE of ANN obtained using the randomly sorted data set, ABC-E is the MSE of ANN obtained using the data set sorted using the ABC algorithm, and AAC-E is the MSE of ANN obtained using the data set sorted using the AAC algorithm.

It is shown that ABC-supported ANN presents the best failure diagnosis performance with a MSE of 0.0107476.

TABLE II. TRAINING AND TEST ERROR AND SUCCESS VALUES FOR ANN, ABC, AND AAC.

	ANN-E	**ABC-E**	**AAC-E**
MSE training	0.00975503	0.00888278	0.015111
MSE2 test	0.0117872	0.0107476	0.0118269

VIII. Conclusions

As in rotor fractures, rotor cracks cause an imbalance in bar currents and ultimately vibrations due to the moment induced in the rotor. This difference can be evaluated by various comparison methods, and it is possible to detect fractures in the rotor bars of the motor by acoustic measurements.

With this study, it was experimentally demonstrated that an ABC-assisted ANN can successfully diagnose rotor fractures. The test results indicate that ABC can improve the performance of the neural network faulty motor detection. If Table II is examined, it is seen that ABC-assisted ANN presents a 9 % improvement in rotor crack detection compared to ANN.

Finally, future work will consider phase current signals and different metaheuristic optimization algorithms in the detection of motor failure.

Conflicts of Interest

The authors declare that they have no conflicts of interest.

References

[1] P. C. M. Lamim Filho, R. Pederiva, and J. N. Brito, "Detection of stator winding faults in induction machines using flux and vibration analysis", *Mechanical Systems and Signal Processing*, vol. 42, nos. 1–2, pp. 377–387, 2014. DOI: 10.1016/j.ymssp.2013.08.033.

[2] A. Bellini, F. Filippetti, C. Tassoni, and G.-A. Capolino, "Advances in diagnostic techniques for induction machines", *IEEE Transactions on Industrial Electronics*, vol. 55, no. 12, pp. 4109–4126, 2008. DOI: 10.1109/TIE.2008.2007527.

[3] A. Glowacz and Z. Glowacz, "Diagnosis of stator faults of the single-phase induction motor using acoustic signals", *Applied Acoustics*, vol. 117, pp. 20–27, 2017. DOI: 10.1016/J.APACOUST.2016.10.012.

[4] P. A. Delgado-Arredondo, D. Morinigo-Sotelo, R. A. Osornio-Rios, J. G. Avina-Cervantes, H. Rostro-Gonzalez, and R. de J. Romero-Troncoso, "Methodology for fault detection in induction motors via sound and vibration signals", *Mechanical Systems and Signal Processing*, vol. 83, pp. 568–589, 2017. DOI: 10.1016/j.ymssp.2016.06.032.

[5] F. M. H. Khater, M. I. A. El-Sebah, M. Osama, and K. S. Sakkoury, "Proposed fault diagnostics of a broken rotor bar induction motor fed from PWM inverter", *Journal of Electrical Systems and Information Technology*, vol. 3, no. 3, pp. 387–397, 2016. DOI: 10.1016/j.jesit.2016.07.004.

[6] A. Abid, M. T. Khan, H. Lang, and C. W. de Silva, "Adaptive system identification and severity index-based fault diagnosis in motors", *IEEE/ASME Transactions on Mechatronics*, vol. 24, no. 4, pp. 1628–1639, 2019. DOI: 10.1109/TMECH.2019.2917749.

[7] B. Asad, T. Vaimann, A. Belachen, A. Kallaste, A. Rassölkin, and M. N. Iqbal, "Broken rotor bar fault detection of the grid and inverter-fed induction motor by effective attenuation of the fundamental component", *IET Electric Power Applications*, vol. 13, no. 12, pp. 2005–20104, 2019. DOI: 10.1049/iet-epa.2019.0350.

[8] D. B. B. de Deus, C. A. N. Sobrinho, F. A. Belo, A. V. Brito, J. G. G. de Souza Ramos, and A. C. Lima-Filho, "Density of maxima approach for broken bar fault diagnosis in low slip and variable load conditions

of induction motors", *IEEE Transactions on Instrumentation and Measurement*, vol. 69, no. 12, pp. 9797–9804, 2020. DOI: 10.1109/TIM.2020.3003107.

[9] T. A. Garcia-Calva, D. Morinigo-Sotelo, A. Garcia-Perez, D. Camarena-Martinez, and R. de J. Romero-Troncoso, "Demodulation technique for broken rotor bar detection in inverter-fed induction motor under non-stationary conditions", *IEEE Transactions on Energy Conversion*, vol. 34, no. 3, pp. 1496–1503, 2019. DOI: 10.1109/TEC.2019.2917405.

[10] C. G. Dias, L. C. da Silva, and W. A. L. Alves, "A histogram of oriented gradients approach for detecting broken bars in squirrel-cage induction motors", *IEEE Transactions on Instrumentation and Measurement*, vol. 69, no. 9, pp. 6968–6981, 2020. DOI: 10.1109/TIM.2020.2975388.

[11] Y. Soleimani, S. M. A. Cruz, and F. Haghjoo, "Broken rotor bar detection in induction motors based on air-gap rotational magnetic field measurement", *IEEE Transactions on Instrumentation and Measurement*, vol. 68, no. 8, pp. 2916–2925, 2019. DOI: 10.1109/TIM.2018.2870265.

[12] A. Elez, S. Car, S. Tvoric, and B. Vaseghi, "Rotor cage and winding fault detection based on machine differential magnetic field measurement (DMFM)", *IEEE Transactions on Industry Application*, vol. 53, no. 3, pp. 3156–3163, 2017. DOI: 10.1109/TIA.2016.2636800.

[13] Y. Gritli, C. Rossi, D. Casadei, F. Filippetti, and G.-A. Capolino, "A diagnostic space vector-based index for rotor electrical fault detection in wound-rotor induction machines under speed transient", *IEEE Transactions on Industrial Electronics*, vol. 64, no. 5, pp. 3892–3902, 2017. DOI: 10.1109/TIE.2017.2652389.

[14] G. M. Joksimovic, J. Riger, T. M. Wolbank, N. Peric, and M. Vašak, "Stator-current spectrum signature of healthy cage rotor induction machines", *IEEE Transactions on Industrial Electronics*, vol. 60, no. 9, pp. 4025–4033, 2013. DOI: 10.1109/TIE.2012.2236995.

[15] H. Keskes and A. Braham, "Recursive undecimated wavelet packet transform and DAG SVM for induction motor diagnosis", *IEEE Transactions on Industrial Informatics*, vol. 11, no. 5, pp. 1059–1066, 2015. DOI: 10.1109/TII.2015.2462315.

[16] A. Naha, A. K. Samanta, A. Routray, and A. K. Deb, "A method for detecting half-broken rotor bar in lightly loaded induction motors using current", *IEEE Transactions on Instrumentation and Measurement*, vol. 65, no. 7, pp. 1614–1625, 2016. DOI: 10.1109/TIM.2016.2540941.

[17] X. F. St-Onge, J. Cameron, S. Saleh, and E. J. Scheme, "A symmetrical component feature extraction method for fault detection in induction machines", *IEEE Transactions on Industrial Electronics*, vol. 66, no. 9, pp. 7281–7298, 2019. DOI: 10.1109/TIE.2018.2875644.

[18] Y. Trachi, E. Elbouchikhi, V. Choqueuse, and M. E. H. Benbouzid, "Induction machines fault detection based on subspace spectral estimation", *IEEE Transactions on Industrial Electronics*, vol. 63, no. 9, pp. 5641–5651, 2016. DOI: 10.1109/TIE.2016.2570741.

[19] Z. Xu, C. Hu, F. Yang, S.-H. Kuo, C.-K. Goh, A. Gupta, and S. Nadarajan, "Data-driven inter-turn short circuit fault detection in induction machines", *IEEE Access*, vol. 5, pp. 25055–25068, 2017. DOI: 10.1109/ACCESS.2017.2764474.

[20] S. K. Ramu, G. C. R. Irudayaraj, S. Subramani, and U. Subramaniam, "Broken rotor bar fault detection using Hilbert transform and neural networks applied to direct torque control of induction motor drive", *IET Power Electronics*, vol. 13, no. 15, pp. 3328–3338, 2020. DOI: 10.1049/iet-pel.2019.1543.

[21] Y. S. Wang, N. N. Liu, H. Guo, and X. L. Wang, "An engine-fault-diagnosis system based on sound intensity analysis and wavelet packet pre-processing neural network", *Engineering Applications of Artificial Intelligence*, vol. 94, art. 103765, 2020. DOI: 10.1016/j.engappai.2020.103765.

[22] R. Bayir and E. Soylu, "Real time determination of rechargeable batteries' type and the state of charge via cascade correlation neural network", *Elektronika ir Elektrotechnika*, vol. 24, no. 1, pp. 25–30, 2018. DOI: 10.5755/j01.eie.24.1.20150.

[23] Z. Xu, X. Mei, X. Wang, M. Yue, J. Jin, Y. Yang, and C. Li, "Fault diagnosis of wind turbine bearing using a multi-scale convolutional neural network with bidirectional long short term memory and weighted majority voting for multi-sensors", *Renewable Energy*, vol. 182, pp. 615–626, 2022. DOI: 10.1016/j.renene.2021.10.024.

[24] D. Karaboga and B. Akay, "A comparative study of artificial bee colony algorithm", *Applied Mathematics and Computation*, vol. 214, no. 1, pp. 108–132, 2009. DOI: 10.1016/j.amc.2009.03.090.

[25] J. A. Freeman and D. M. Skapura, *Neural Networks: Algorithms, Applications, and Programming Techniques*. Reading, Mass., Addison-Wesley Publishing Company, 1992, ch. 3.

[26] D. Karaboga and B. Basturk, "On the performance of artificial bee colony (ABC) algorithm", *Applied Soft Computing*, vol. 8, no. 1, pp. 687–697, 2008. DOI: 10.1016/j.asoc.2007.05.007.

[27] R. S. Jadon and U. Dutta, "Modified ant colony optimization algorithm with uniform mutation using self-adaptive approach", *International Journal of Computer Applications*, vol. 74, no. 13, pp. 5–8, 2013. DOI: 10.5120/12943-9931.

[28] W. Gao, "New ant colony optimization algorithm for the travelling salesman problem", *International Journal of Computational Intelligence Systems*, vol. 13, no. 1, pp. 44–55, 2020. DOI: 10.2991/ijcis.d.200117.001.